J|A|C|S ARTICLES

Published on Web 04/29/2010

Low-Dimensional Structure and Magnetism of the Quantum Antiferromagnet $Rb_4Cu(MoO_4)_3$ and the Structure of $Rb_4Zn(MoO_4)_3$

Rieko Ishii,[§] Dixie Gautreaux,[†] Keisuke Onuma,[#] Yo Machida,[§,#] Yoshiteru Maeno,[#] Satoru Nakatsuji,[§] and Julia Y. Chan*[,†]

Department of Chemistry, Louisiana State University, Baton Rouge, Louisiana 70803, Institute for Solid State Physics, University of Tokyo, Kashiwa 277-8581, Japan, and Department of Physics, Kyoto University, Kyoto 606-8502, Japan

Received January 5, 2010; E-mail: jchan@lsu.edu

Abstract: Single crystals of the quantum low-dimensional antiferromagnet $Rb_4Cu(MoO_4)_3$ and the nonmagnetic analogue $Ru_4Zn(MoO_4)_3$ have been synthesized by a flux-growth method. Detailed structural studies indicate that the Cu(II)−O network separated by a MoO_4 layer has a strongly anisotropic hybridization along the *a*-axis, forming a quasi-one-dimensional (1-d) chain of Cu(II) $S = 1/2$ spins. Furthermore, our low-temperature thermodynamic measurements have revealed that a quantum paramagnetic state with Wilson ratio ~2 remains stable down to at least 0.1 K, 100 times lower than the intrachain antiferromagnetic coupling scale. The low-temperature magnetic and thermal properties are found to be consistent with theoretical predictions made for a 1-d network of $S = 1/2$ spins.

Introduction

Low-dimensional spin systems have received considerable attention because of the possible emergence of novel magnetism such as quantum critical phenomena,[1] Haldane gap formation,[2−4] and field-induced Bose−Einstein condensation.[5] Quantum fluctuations enhanced by low dimensionality may suppress magnetic ordering and give rise to a variety of exotic phenomena. In order to understand the role of quantum fluctuations in low-dimensional spin systems, it is important to explore its phenomenology in simple and well-controlled model systems.

Oxides containing Cu(II) ions have provided a number of model systems of low-dimensional magnets with $S = 1/2$. The quasi-two-dimensional (2-d) La_2CuO_4,[6] the parent compound of the high-T_c cuprates, is a quantum Heisenberg antiferromagnet on a square lattice, and $SrCu_2(BO_3)_2$[7−9] is a quantum dimer system on a Shastry−Shoutherland lattice.[10] One-dimensional spin chain systems in copper oxides also provide interesting ground states. For example, an antiferromagnetic Heisenberg model with $S = 1/2$ spins is theoretically expected to remain disordered down to $T = 0$ K without forming any long-range order owing to the quantum fluctuations. Instead, a quantum critical state should appear because of divergent spin−spin correlation length as temperature goes to zero. In this quantum spin liquid state, an elementary excitation called spinon emerges, which may be described by a traveling domain wall.[11] Despite such theoretical understanding, the model compounds of such quasi-1-d magnets are still scarce, and thus the study of the quantum critical phase is important. In addition, such 1-d chain magnets hitherto investigated experimentally often exhibit long-range ordering due to finite interchain interactions. Another example, Sr_2CuO_3, is one of the most studied quasi-1-d $S = 1/2$ antiferromagnets, and in spite of the large exchange coupling $J \approx 1300$ K, neutron scattering measurements show that this has three-dimensional long-range ordering below $T_N \approx 5.4$ K, indicating a rather small coupling ratio $J'/J \approx 10^{-5}$, where J' is the interchain coupling.[12,13] Another prototypical compound is copper benzoate, $Cu(C_6H_5COO)\cdot 3H_2O$, with $J = 8.6$ K, and for this magnet, very interestingly, no long-range order is observed down to 0.02 K by the muon spin relaxation measurement.[14] $Sr_2Cu(PO_4)_2$ is considered one of the best realizations of a 1-d Heisenberg chain in terms of the small ratio J'/J, and

[§] University of Tokyo.
[†] Louisiana State University.
[#] Kyoto University.

(1) Sachdev, S. *Quantum Phase Transition*; Cambridge University Press: New York, 1999.
(2) Haldane, F. D. M. *Phys. Rev. Lett.* **1983**, *50*, 1153–1156.
(3) Yamashita, M.; Ishii, T.; Matsuzaka, H. *Coord. Chem. Rev.* **2000**, *198*, 347–366.
(4) Affleck, I. *J. Phys. Condensed Matter* **1989**, *1*, 3047–3072.
(5) Giamarchi, T.; Ruegg, C.; Tchernyshyov, O. *Nature Phys.* **2008**, *4*, 198–204.
(6) Anderson, P. W. *Science* **1987**, *235*, 1196–1198.
(7) Kageyama, H.; Yoshimura, K.; Stern, R.; Mushnikov, N. V.; Onizuka, K.; Kato, M.; Kosuge, K.; Slichter, C. P.; Ueda, Y. *Phys. Rev. Lett.* **1999**, *82*, 3168–3171.
(8) Knetter, C.; Muller-Hartmann, E.; Uhrig, G. S. *J. Phys. Condensed Matter* **2000**, *12*, 9069–9083.
(9) Kageyama, H.; Onizuka, K.; Yamauchi, T.; Ueda, Y.; Hane, S.; Mitamura, H.; Goto, T.; Yoshimura, K.; Kosuge, K. *J. Phys. Soc. Jpn.* **1999**, *68*, 1821–1823.
(10) Shastry, B. S.; Sutherland, B. *Physica B & C* **1981**, *108*, 1069–1070.
(11) *One-dimensional magnetism*; Mikeska, H. J., Kolezhuk, A. K., Eds.; Springer: Berlin, 2004; Vol. 645.
(12) Kojima, K. M.; Fudamoto, Y.; Larkin, M.; Luke, G. M.; Merrin, J.; Nachumi, B.; Uemura, Y. J.; Motoyama, N.; Eisaki, H.; Uchida, S.; Yamada, K.; Endoh, Y.; Hosoya, S.; Sternlieb, B. J.; Shirane, G. *Phys. Rev. Lett.* **1997**, *78*, 1787–1790.
(13) Motoyama, N.; Eisaki, H.; Uchida, S. *Phys. Rev. Lett.* **1996**, *76*, 3212–3215.
(14) Asano, T.; Nojiri, H.; Higemoto, W.; Koda, A.; Kadono, R.; Ajiro, Y. *J. Phys. Soc. Jpn.* **2002**, *71*, 594–598.

first-principle calculations have been employed to make a comparison between experimental results and theoretical models.[15] Several years ago, the synthesis and magnetic characterization of the first structurally perfect copper hydroxide chloride mineral, $Zn[Cu_3(OH)_6Cl_2]$, with spin of $S = 1/2$ Kagomé antiferromagnet, was realized.[16] More recently, a metal−organic hybrid material, Cu(1,3-bdc) (1,3-bdc =1,3-benzenedicarboxylate), has also been shown to exhibit a novel, structurally perfect $S = 1/2$ Kagomé antiferromagnet, which has opened up an area for the study of quantum disordered phases.[17]

Molybdate compounds exhibit a wide variety of properties, including catalytic gas-phase oxidation of organic compounds, magnetism, magnetoresistance, and ferroelectricity. When they contain a MoO_4 tetrahedral unit, 4d transition metal Mo^{6+} ions form a closed shell with $S = 0$. Thus, a corner-sharing MoO_4 layer may serve as a nonmagnetic block to separate magnetic ions and to construct a low-dimensional network of spins. A well-known example is $RbFe(MoO_4)_2$,[18] a model system of a quasi-2-d triangular antiferromagnet with $S = 5/2$. It shows a variety of interesting phenomena, such as low-temperature multiferroic properties and a 1/3 magnetic plateau phase with a magnetic field. In the plateau phase, an increase of magnetization with applied magnetic field is suppressed due to its characteristic spin structure, such as an "up-up-down" state.[19]

In our search for low-dimensional quantum antiferromagnets ($S = 1/2$), we have succeeded in growing high-quality single crystals of $Rb_4Cu(MoO_4)_3$ and $Rb_4Zn(MoO_4)_3$. In previous literature reports, three types of the temperature-dependent structures were found, indicating that $Rb_4Cu(MoO_4)_3$ undergoes two temperature-dependent structural phase transitions.[20] The structure was reported to adopt a hexagonal cell ($a = 6.15$ Å, $c = 23.23$ Å) above room temperature, an orthorhombic phase ($a = 6.074$ Å, $b = 21.20$ Å, $c = 23.21$ Å) at room temperature, and a monoclinic cell ($a = 5.999$ Å, $b = 21.08$ Å, $c = 23.03$ Å; $\gamma = 90.06°$) around 103 K. A similar orthorhombic lattice was also reported for β-$Rb_4Zn(MoO_4)_3$, which adopts the $Pn2_1a$ space group with cell dimensions of $a = 10.90$ Å, $b = 22.42$ Å, and $c = 6.271$ Å; however, no other structural information was reported for this compound.[20] In this article, we report the synthesis, full structure determination, and physical properties of the quantum antiferromagnet $Rb_4Cu(MoO_4)_3$ and its nonmagnetic reference material $Rb_4Zn(MoO_4)_3$. We also report the magnetic and thermal properties of $Rb_4Cu(MoO_4)_3$ as a new candidate quasi-1-d Heisenberg quantum antiferromagnet.

Experimental Section

Synthesis. The polycrystalline samples of $Rb_4Cu(MoO_4)_3$ and $Rb_4Zn(MoO_4)_3$ are synthesized via ceramic reaction method according to the chemical reaction,

$$2Rb_2CO_3 + MO + 3MoO_3 \rightarrow Rb_4M(MoO_4)_3 + 2CO_2\uparrow \quad (M = Cu, Zn)$$

Here, because Rb_2CO_3 is highly hygroscopic, it was necessary to dehydrate by heating at 300 °C for over 3 h before grinding. The mixture was pressed into a pellet and calcined at 480 °C for 40 h. This procedure was repeated three times until a single phase was obtained. The single crystals were grown by using $Rb_2Mo_2O_7$ as flux. We used the polycrystalline sample as a charge, and the charge−flux molar ratio was 1:1. After the melt solutions were kept at oxygen atmosphere in a fused-silica tube at 590−600 °C for 40 h, they were cooled to 500 °C at 1 deg/h. Greenish transparent hexagonal cylindrical $Rb_4Cu(MoO_4)_3$ crystals and colorless transparent thin crystals of $Rb_4Zn(MoO_4)_3$ were obtained. There were no impurities in the samples grown, as confirmed by X-ray powder diffraction.

Structure Determination. The single-crystal X-ray diffraction data of $Rb_4Cu(MoO_4)_3$ and $Rb_4Zn(MoO_4)_3$ were collected at 298 and 100 K, respectively. Due to the extremely hygroscopic nature of the samples, the crystals were placed in Paratone-N oil to protect the sample from exposure to air and moisture. A crystal with approximate dimensions of $0.05 \times 0.10 \times 0.125$ mm^3 was mounted onto a glass fiber of the goniometer and placed on a Nonius Kappa CCD X-ray diffractometer (Mo Kα = 0.71073 Å). Temperature was regulated with a cooled nitrogen gas stream produced by an Oxford cryostream cooler. The unit cell parameters were determined from images taken at a rotation of 15°φ. Initial structural models were solved by SIR97 and refined by direct methods against F^2 by full-matrix least-squares techniques using SHELXL97.[21] The data were corrected for absorption, and the displacement parameters were refined as anisotropic. Structural refinement data for $Rb_4Cu(MoO_4)_3$ and $Rb_4Zn(MoO_4)_3$ are given in Table 1, and the atomic parameters are given in Tables 2 and 3 for $Rb_4Cu(MoO_4)_3$ and $Rb_4Zn(MoO_4)_3$, respectively. The lattice dimensions of $Rb_4Cu(MoO_4)_3$ are similar to those of the orthorhombic compound $K_4Zn(MoO_4)_3$, which crystallizes in the space group $P2_12_12_1$.[22,23] An attempt was made to refine the structural model of $Rb_4Cu(MoO_4)_3$ using the structural information from the $K_4Zn(MoO_4)_3$, and although an acceptable R-value was obtained, the atomic displacement parameters for

Table 1. Crystallographic Data for $Rb_4Cu(MoO_4)_3$ and $Rb_4Zn(MoO_4)_3$

	Crystal Data	
formula	$Rb_4Cu(MoO_4)_3$	$Rb_4Zn(MoO_4)_3$
space group	*Pnma*	*Pbca*
a (Å)	10.581(2)	12.485(2)
b (Å)	23.213(4)	10.8750(10)
c (Å)	6.078(1)	22.2660(10)
V (Å^3)	1492.9(5)	3023.2(6)
Z	4	8
crystal dimens (mm^3)	$0.075 \times 0.15 \times 0.175$	$0.05 \times 0.10 \times 0.125$
temperature (K)	298	100
density (g cm^{-3})	3.939	3.898
θ range (°)	3.46−30.02	2.45−30.02
μ (mm^{-1})	16.872	16.843
	Data Collection and Refinement	
collected reflns	3948	8235
unique reflns	1582	2922
R_{int}	0.0295	0.0535
h	$-14 \le h \le 14$	$-17 \le h \le 17$
k	$-32 \le k \le 32$	$-15 \le k \le 15$
l	$-8 \le l \le 8$	$-31 \le l \le 31$
$\Delta\rho_{max}$ (e Å^{-3})	2.333	2.495
$\Delta\rho_{min}$ (e Å^{-3})	−1.226	−1.940
GoF	1.052	1.03
extinction coefficient	0.00084(11)	0.000134(18)
$R_1(F)$ for $F_o^2 > 2\sigma(F_o^2)^a$	0.0508	0.0456
$R_w(F_o^2)^b$	0.1103	0. 0919

^{a} $R_1(F) = \sum||F_o| - |F_c||/\sum|F_o|$. ^{b} $R_w(F_o^2) = \sum[w(F_o^2 - F_c^2)^2]/\sum[w(F_o^2)^2]^{1/2}$.

(15) Johannes, M. D.; Richter, J.; Drechsler, S.-L.; Rosner, H. *Phys. Rev. B* **2006**, *74*, 174435.
(16) Shores, M. P.; Nytko, E. A.; Bartlett, B. M.; Nocera, D. G. *J. Am. Chem. Soc.* **2005**, *127*, 13462–13463.
(17) Nytko, E. A.; Helton, J. S.; Muller, P.; Nocera, D. G. *J. Am. Chem. Soc.* **2008**, *130*, 2922–2923.
(18) Svistov, L. E.; Smirnov, A. I.; Prozorova, L. A.; Petrenko, O. A.; Demianets, L. N.; Shapiro, A. Y. *Phys. Rev. B* **2003**, *67*, 094434.
(19) Miyashita, S. *J. Phys. Soc. Jpn.* **1986**, *55*, 3605–3617.
(20) Trunov, K.; Efremov, V. A.; Velikodnyi, Y. A. *Crystal Chemistry and Properties of Double Molybdates and Tungstates*; Nauka: Leningrad, 1986 [in Russian].

Table 2. Atomic Coordinates and Anisotropic Displacement Parameters for $Rb_4Cu(MoO_4)$

atom	Wyckoff site	*x*	*y*	*z*	U_{eq} (Å^2)[a]	occupancy
Rb1	8*d*	0.33338(8)	0.47125(3)	0.50086(12)	0.0258(2)	1
Rb2	8*d*	0.33349(10)	0.66056(3)	0.47298(16)	0.0378(2)	1
Mo1	8*d*	0.00050(6)	0.59262(2)	0.50809(10)	0.01809(17)	1
Mo2	8*d*	0.16952(16)	0.73000(6)	0.9616(3)	0.0285(2)	0.5
Cu1	4*c*	0.00041(14)	1/4	0.5088(2)	0.0223(3)	1
O1	8*d*	0.4181(6)	0.5647(3)	0.2159(10)	0.0361(15)	1
O2	4*c*	0.4590(12)	1/4	0.603(3)	0.075(4)	1
O3	8*d*	0.4280(7)	0.5690(3)	0.7497(11)	0.0410(16)	1
O4	8*d*	−0.0003(8)	0.6692(3)	0.4940(14)	0.054(2)	1
O5	8*d*	0.1542(6)	0.5672(3)	0.5002(11)	0.0388(15)	1
O6	4*c*	0.8410(11)	1/4	0.325(2)	0.057(3)	1
O7	4*c*	0.6865(11)	1/4	0.927(2)	0.070(4)	1
O8	8*d*	0.1736(13)	0.6559(5)	0.983(2)	0.044(4)	0.5

[a] U_{eq} is defined as one-third of the trace of the orthogonalized U_{ij} tensor.

Table 3. Atomic Positions and Displacement Parameters for $Rb_4Zn(MoO_4)_3$

atom	Wyckoff site	*x*	*y*	*z*	U_{eq} (Å^2)[a]
Rb1	8*c*	0.62709(5)	0.91860 (6)	0.97183(3)	0.01378(15)
Rb2	8*c*	0.87567(5)	0.08440(6)	0.03151(3)	0.01385(15)
Rb3	8*c*	0.10545(6)	0.57003(6)	0.83948(3)	0.01477(15)
Rb4	8*c*	0.62453(5)	0.59903(6)	0.84265(3)	0.01486(16)
Zn1	8*c*	0.32067(7)	0.71724(7)	0.75429(3)	0.01259(18)
Mo1	8*c*	0.37662(4)	0.74717(5)	0.90582(2)	0.00993(13)
Mo2	8*c*	0.87294(4)	0.75407(5)	0.90704(2)	0.01007(13)
Mo3	8*c*	0.37491(5)	0.42223(5)	0.73384(3)	0.01156(14)
O1	8*c*	0.3690(4)	0.7428(4)	0.6740(2)	0.0205(11)
O2	8*c*	0.4986(4)	0.4614(4)	0.7629(2)	0.0165(10)
O3	8*c*	0.3980(4)	0.7525(4)	0.82513(19)	0.0167(11)
O4	8*c*	0.5121(4)	0.1802(4)	0.9333(2)	0.0188 (11)
O5	8*c*	0.2808(4)	0.5400(4)	0.75474(19)	0.0168(10)
O6	8*c*	0.1704(4)	0.7760(4)	0.7622(2)	0.0178(10)
O7	8*c*	0.2594(4)	0.6681(5)	0.9229(2)	0.0224(12)
O8	8*c*	0.3683(4)	0.8969(4)	0.9333(2)	0.0201(11)
O9	8*c*	0.3833(4)	0.4173(4)	0.65647(19)	0.0195(11)
O10	8*c*	0.4851(4)	0.6700(4)	0.9381(2)	0.0206(11)
O11	8*c*	0.6227(4)	0.4084(4)	0.92981(19)	0.0167(11)
O12	8*c*	0.7585(4)	0.6840(4)	0.93782(19)	0.0174(11)

[a] U_{eq} is defined as one-third of the trace of the orthogonalized U_{ij} tensor.

multiple atoms were large and not well-behaved. Also, the intensities of the observed structure factors were generally higher than the calculated values, indicating either a twinned or incorrect absolute structure. These differences all contribute to choosing the higher symmetry *Pnma* model over the published $P2_12_12_1$ model, and this is not unexpected, given that the difference between the two structure types is the transition metal coordination environment, where the Zn in $K_4Zn(MoO_4)_3$ adopts a tetrahedral bonding environment while the Cu in $Rb_4Cu(MoO_4)_3$ resides in a distorted square planar environment.

Magnetic and Thermal Properties. We measured the magnetization *M* down to 1.9 K under a magnetic field $\mu_0 H$ up to 7 T with a MPMS SQUID magnetometer to investigate the magnetic properties of $Rb_4Cu(MoO_4)_3$. The specific heat *C* was measured by the thermal relaxation method using a He^3 and/or dilution refrigerator down to 0.1 K for $Rb_4Cu(MoO_4)_3$ and using a He^3 refrigerator down to 0.4 K for $Rb_4Zn(MoO_4)_3$.

Results and Discussion

Crystal Structure of $Rb_4Cu(MoO_4)_3$. $Rb_4Cu(MoO_4)_3$ adopts the *Pnma* space group with lattice dimensions of $a = 10.581(2)$ Å, $b = 23.213(4)$ Å, and $c = 6.078(1)$ Å, and selected bond distances and angles are provided as Supporting Information. $Rb_4Cu(MoO_4)_3$ is shown in Figure 1, and the structure consists of distorted square planar CuO_4 bonded to two slightly distorted MoO_4 tetrahedral units in the *c*-direction. Mo1 adopts a slightly distorted tetrahedral environment, with interatomic distances ranging from 1.731(6) to 1.780(6) Å. Mo2 is also slightly distorted in a tetrahedral environment, with interatomic distances ranging from 1.674(13) to 1.805(12) Å. Mo2 is disordered, with an occupancy of 0.5. Rb1 is coordinated to 10 oxygen atoms, with bond distances ranging from 2.905(6) to 3.294(7) Å. Rb2 is coordinated to six oxygen atoms, with bond distances ranging from 2.862(6) to 3.205(11) Å.

Figure 2 shows the 1-d Cu chains with Cu−O distances ranging from 1.876(6) to 2.023(11) Å and O−Cu−O angles of 157.6(5)° and 179.0(5)°. Cu superexchange is possible because the layers of Cu subunits are connected by the MoO_4 subunits. There are two types of superexchange paths, *J* and *J′*, as shown in Figure 2a. The distorted square pyramid CuO_5 environment should stabilize a lone pair in the $d_{x^2-y^2}$ orbital, as also seen in other oxide structures such as La_2CuO_4.[6] Along the superexchange path *J*, the disordered, slightly distorted MoO_4 tetrahedral units link the CuO_5 subunits. This path includes the strong σ bond between the $d_{x^2-y^2}$ orbital of Cu^{2+} and the $p_{x,y}$ orbitals of O^{2-}. On the other hand, the main magnetic link along the superexchange path *J′* must involve the coupling between the Cu^{2+} ion and the O^{2-} ion at the apical site of the square pyramid CuO_5. This coupling should be weak because of (1) the long Cu−O distance of 2.4 Å and (2) the almost orthogonal spatial configuration for the relation between the $d_{x^2-y^2}$ orbital of Cu^{2+} and the p_z orbital of O^{2-}, which results in a negligibly small superexchange bond *J′* in comparison with *J*. To illustrate this, we draw the local coordination and the Cu^{2+} $d_{x^2-y^2}$ and the O^{2-} p_z orbitals as shown in Figure 2b. Thus, one localized electron in the anisotropic $d_{x^2-y^2}$ orbital is likely to form a strong superexchange path *J* along the *a*-axis and organize a 1-d spin chain. This 1-d spin coupling is counterintuitive, because the material has an apparently layered structure where a Cu^{2+} ion is densely distributed to form a distorted triangular lattice in a 2-d layer on the *ac* plane, separated by Rb^+ and MoO_4 block layers. In this system, however, the arrangement of the anisotropic hybridization between Cu 3d and O 2p orbitals stabilizes the 1-d chain of Cu−O−Mo−O−Cu along the *a*-axis, as shown in Figure 2a. Although this orthorhombic structure is similar to that of other molybdates, it actually differs significantly in the geometry of the transition metal atom, as discussed previously.

(21) Sheldrick, G. M. *SHELXL97*; University of Gottingen: Germany, 1997.
(22) Gicquel-Mayer, C.; Mayer, M.; Perez, G. *Rev. Chem. Miner.* **1980**, *17*, 445–457.
(23) Gicquel-Mayer, C.; Mayer, M.; Perez, G. *C. R. Acad. Sci. Paris* **1976**, *283*, 533–535.

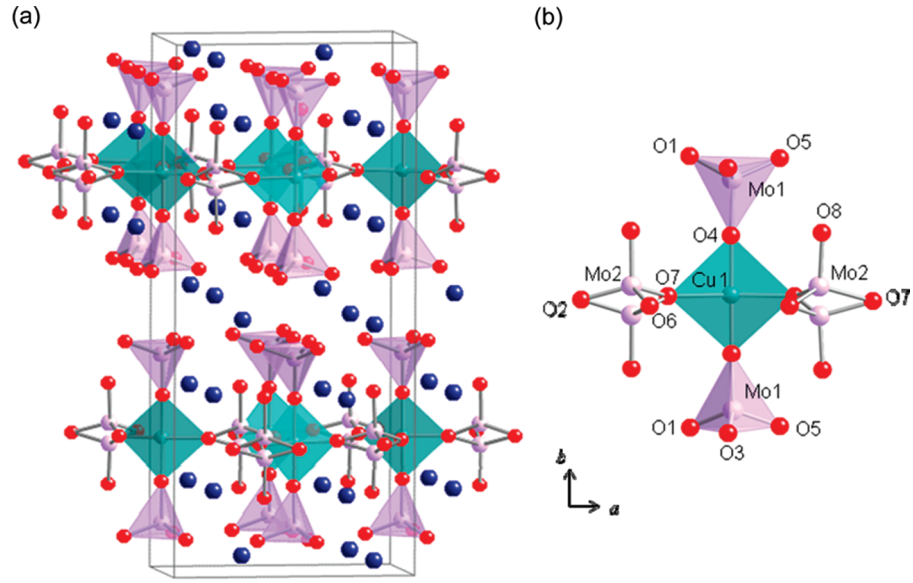

Figure 1. (a) Crystal structure of $Rb_4Cu(MoO_4)_3$ as viewed down the *c*-axis, where the blue, green, purple, and red spheres refer to Rb, Cu, Mo, and O atoms, respectively. (b) Distorted Cu square planar environment of $Rb_4Cu(MoO_4)_3$.

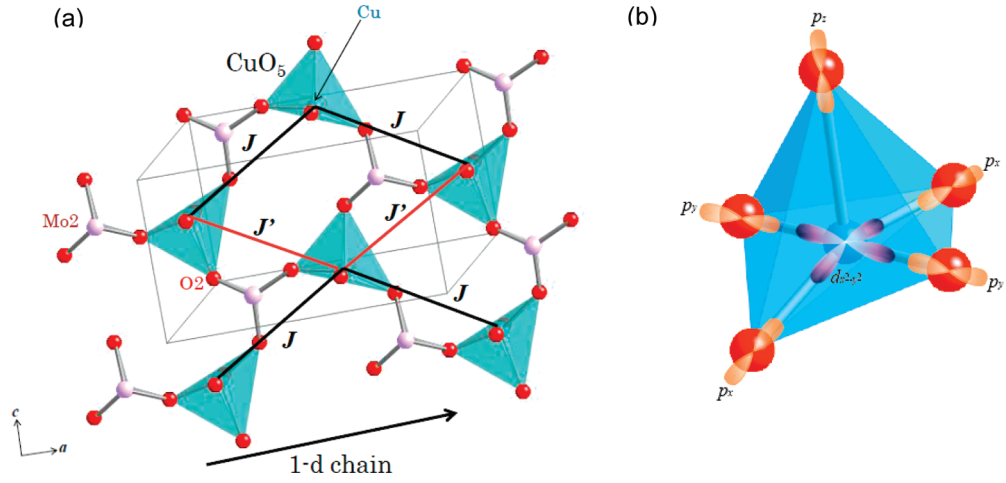

Figure 2. (a) View of the Cu 1-d chains and their bonding environment. Both *J* and *J*′ indicate two types of near-neighbor superexchange couplings between $S = 1/2$ spins at the Cu^{2+} ion, connected through Cu−O−Mo−O−Cu paths. The longer Cu−O2 apical contacts are not shown for clarity. (b) The local coordination of CuO_5, showing the $d_{x^2-y^2}$ orbital of Cu^{2+} and the p_x, p_y, and p_z orbitals of O^{2-}. For simplicity, we show d and p orbitals for the ideal CuO_4 square coordination, neglecting small local distortions.

Crystal Structure of $Rb_4Zn(MoO_4)_3$. The structure of $Rb_4Zn(MoO_4)_3$ crystallizes in the orthorhombic space group *Pbca* (No. 61) and adopts a new structure type with lattice parameters of $a = 12.485(2)$ Å, $b = 10.8750(10)$ Å, and $c = 22.2660(10)$ Å, as shown in Figure 3. Selected bond distances and angles are provided as Supporting Information. The structure consists of slightly distorted ZnO_4 tetrahedral units surrounded by four slightly less distorted MoO_4 tetrahedra. The Zn tetrahedra form chains with Mo3 tetrahedra along the *b*-axis and are capped by Mo1 and Mo3 tetrahedra in the *c*-direction. The new $Rb_4Zn(MoO_4)_3$ structure type is similar to other double molybdates such as $Rb_4Mn(MoO_4)_3$;[24] however, one notable difference between the Zn analogue and the hexagonal $Rb_4Mn(MoO_4)_3$ is the coordination environment of the transition metal, where the Mn analogue consists of a Mn trigonal bipyramid while the Zn analogue contains slightly distorted Zn tetrahedra.[25,26] The structure of $Rb_4Zn(MoO_4)_3$ is also reminiscent of the orthorhombic $K_4Zn(MoO_4)_3$ ($P2_12_12_1$ space group).[22,23] Although Zn adopts a tetrahedral environment in both analogues, the orthorhombic $K_4Zn(MoO_4)_3$ structure type contains disordered MoO_4 subunits, not observed in the Rb analogue.

The O−Mo−O angles in the tetrahedral subunits range from 107.9(2)° to 110.9(2)° for Mo1, 108.5(2)° to 110.7(2)° for Mo2, and 108.2(2)° to 111.5(2)° for Mo3, indicating a slight deviation from the expected angle of 109.5°. The O−Zn−O angles range from 94.28(19)° to 126.3(2)° for the ZnO_4 tetrahedra, showing more distortion than the MoO_4 units. The distances are consistent with the ionic radii of Rb^+, Zn^{2+}, and Mo^{6+} as well as the distances in the known $K_4Zn(MoO_4)_3$ structure.[22,23,27]

(24) Ishii, R.; Tanaka, S.; Onuma, K.; Nambu, Y.; Tokunaga, M.; Sakakibara, T.; Kawashima, N.; Maeno, Y.; Broholm, C.; Gautreaux, D. P.; Chan, J. Y.; Nakatsuji, S. arXiv:0912.4796, submitted 24 Dec 2009 (http://arxiv.org/abs/0912.4796).

(25) Klevtsova, R. F.; Solodovnikov, S. F.; Klevtsov, P. V. *Izv. Akad. Nauk SSSR Ser. Fiz.* **1986**, *50*, 353–355.

(26) Solodovnikov, S. F.; Klevtsova, R. F.; Glinskaya, L. A.; Klevtsov, P. V. *Sov. Phys. Crystallogr.* **1988**, *33*, 820–824.

(27) Shannon, R. D. *Acta Crystallogr.* **1976**, *32A*, 751–767.

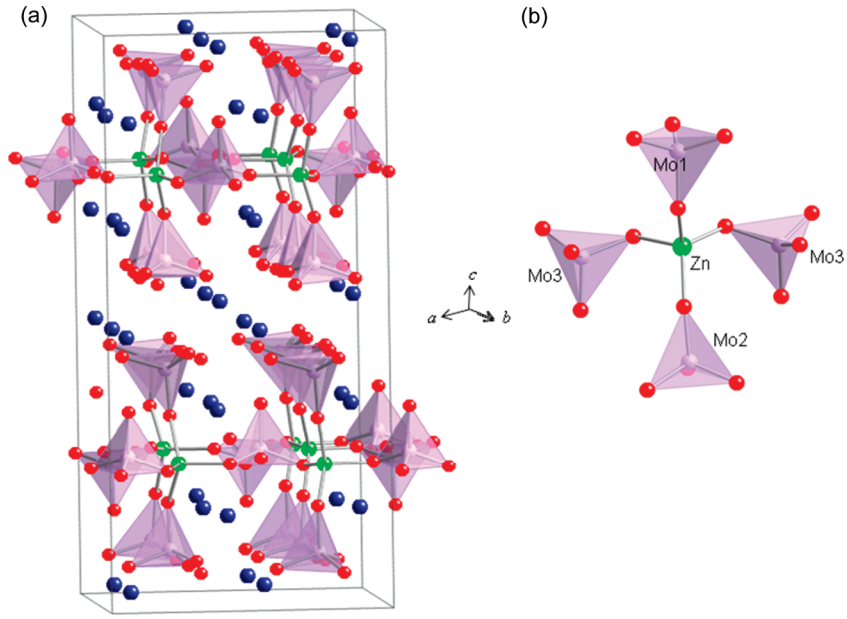

Figure 3. (a) Crystal structure of $Rb_4Zn(MoO_4)_3$ as viewed down the *a*-axis, where the blue, green, purple, and red spheres refer to Rb, Zn, Mo, and O atoms, respectively. (b) Zn bonding environment of $Rb_4Zn(MoO_4)_3$.

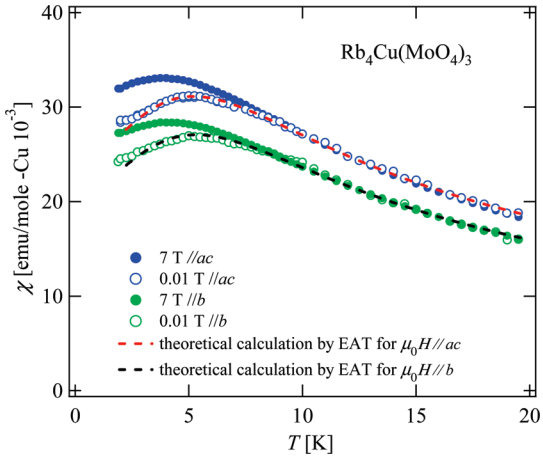

Figure 4. Temperature dependence of the magnetic susceptibilities of $Rb_4Cu(MoO_4)_3$ below 40 K. Blue (green) solid and open circles show magnetization $\mu_0H\|ac$ (*b*) at 7 and 0.01 T, respectively. There is no hysteresis between results obtained by zero-field-cooled and field-cooled measurements. The red (black) dashed line shows the result of the fitting by the theoretical calculation by Eggert, Affleck, and Takahashi[29] using the anisotropic *g*-values and the antiferromagnetic coupling *J* estimated from the Curie−Weiss analyses (see text).

Physical Properties of $Rb_4Cu(MoO_4)_3$. The one-dimensional nature structurally expected for the exchange interaction between neighboring Cu^{2+} ions with $S = 1/2$ has been confirmed by comprehensive measurements, including the temperature dependence of the susceptibility and the specific heat and the magnetization process under magnetic fields for $Rb_4Cu(MoO_4)_3$. The temperature dependence of the magnetic susceptibilities at $\mu_0H = 0.01$ and 7 T for $\mu_0H\|ac$ and $\mu_0H\|b$ have a broad peak at 5 K, which is characteristic of the $S = 1/2$ 1-d spin chain system as we will compare them with theoretical calculation below, and shows no anomaly indicative of a phase transition down to 1.9 K (Figure 4). There is no difference in the zero-field-cooled and field-cooled results at 0.01 T. Data were corrected for the diamagnetism of the core electron in $Rb_4Cu(MoO_4)_3$, $\chi_{dia} = -256 \times 10^{-6}$ emu/mol.[28] The difference between two susceptibilities for $\mu_0H\|ac$ and $\mu_0H\|b$ is attributable to the anisotropy of the *g*-value and the Van Vleck's paramagnetism. We fitted the χ data assuming that $\chi = \chi_0 + C/(T - \Theta_W)$ for 40−300 K and obtained the effective magnetic moment p_{eff}, *g*-value, Weiss temperature Θ_W, and χ_0 as shown in Table 4. The Weiss temperatures are both negative and indicate the antiferromagnetic interaction between neighboring Cu^{2+} ions. The constant term $\chi_0 \sim 2.0 \times 10^{-4}$ emu/mol for $\mu_0H\|ac$ and 3.2×10^{-4} emu/mol for $\mu_0H\|b$ are most likely due to the Van Vleck's paramagnetism by the orbital hybridization. p_{eff} for $\mu_0H\|b$ is close to the theoretical value 1.73 μ_B for $S = 1/2$. On the other hand, p_{eff} for $\mu_0H\|ac$ is larger than 1.73 μ_B and is ascribable to spin−orbit coupling. The exchange interaction can be estimated to be $J \approx 10.0$ K by using the relation $\Theta_w = -[zs(s + 1)J]/3$, where $z = 2$ is the number of nearest-neighbor magnetic ions. Using the above anisotropic *g*-values and the antiferromagnetic coupling constant *J*, now we compare our $\chi(T)$ results with the theoretical calculation of $S = 1/2$ antiferromagnetic Heisenberg 1-d spin chain system with high accuracy obtained by Eggert, Affleck, and Takahashi in Figure 4.[29] The agreement is rather good except for a slight deviation at low temperatures below the peak temperature. The slight positive deviation in comparison with theory may come from weak interchain coupling, as will be discussed below.

Figure 5 shows the magnetization measured at 2 K for $\mu_0H\|ac$ and $\mu_0H\|b$. Magnetization curves have a convex downward

Table 4. Magnetic Effective Moment p_{eff}, *g*-Value, Weiss Temperature Θ_W, and Uniform Susceptibility χ_0 in $Rb_4Cu(MoO_4)_3$, Obtained by Curie−Weiss Fitting

$Rb_4Cu(MoO_4)_3$	$\mu_0H\|ac$	$\mu_0H\|b$
p_{eff}	1.91	1.79
g	2.21	2.07
Θ_W (K)	−5.01	−5.15
χ_0 (emu/mol)	2.00×10^{-4}	3.18×10^{-4}

(28) Selwood, P. W. *Magnetochemistry*; Interscience: New York, 1956.
(29) Eggert, S.; Affleck, I.; Takahashi, M. *Phys. Rev. Lett.* **1994**, *73*, 332–335.

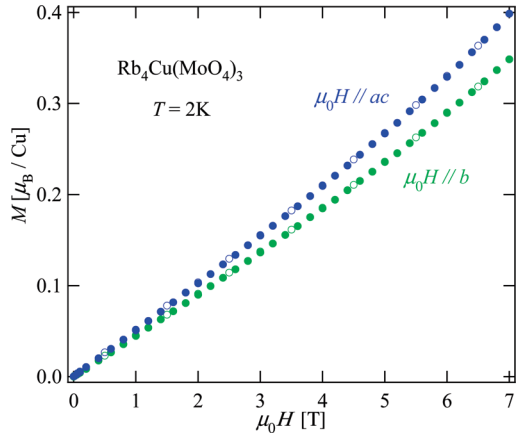

Figure 5. Field dependence of the magnetization of a single crystal of $Rb_4Cu(MoO_4)_3$ up to 7 T, measured at 2 K for μ_0H||b and μ_0H||ac. Solid and open circles show the up-sweep and down-sweep results, respectively.

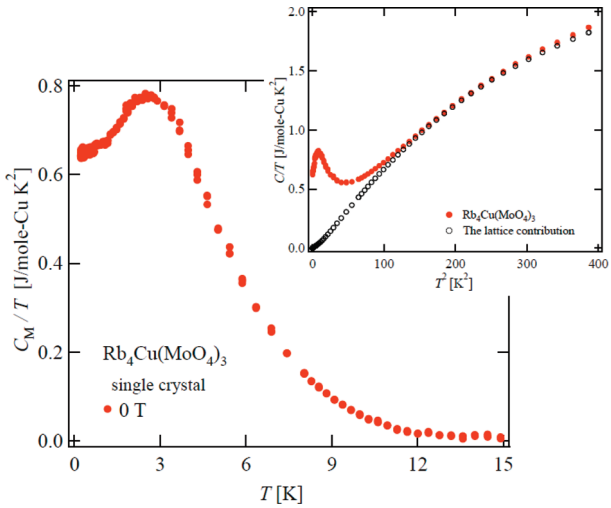

Figure 6. Temperature dependence of the magnetic specific heat of $Rb_4Cu(MoO_4)_3$. Red solid circles are the results at 0 T. Inset: Temperature dependence of the total specific heat of $Rb_4Cu(MoO_4)_3$ (red) and the lattice contribution to the specific heat of $Rb_4Zn(MoO_4)_3$ (black). The latter is estimated from the specific heat of the nonmagnetic analogue $Rb_4Zn(MoO_4)_3$ by obtaining thermal variations of its Debye temperature using the Debye equation.[36]

curvature, as often seen in $S = 1/2$ systems.[30] Normally, M shows the convex upward dependence of H, obeying the Brillouin function, when there is no magnetic correlation. Meanwhile, if the antiferromagnetic correlation develops, M is linear over a wide range of H. However, in $S = 1/2$ systems, if the antiferromagnet correlation develops, spin singlet pairs are partially formed, and the average length of spins shortens, owing predominantly to quantum fluctuations. Because the length of spins elongates again with applied field, the slope of the magnetization curve is enhanced by applying field. We have also carried out specific heat measurements for $Rb_4Cu(MoO_4)_3$ under various fields. Figure 6 shows the temperature dependence of the magnetic specific heat C_M at $\mu_0H = 0$ T. C_M was estimated by subtracting the lattice contribution, which was estimated using the total specific heat of the nonmagnetic analogue $Rb_4Zn(MoO_4)_3$. $Rb_4Zn(MoO_4)_3$ does not have completely the same structure, but it is similar and provides the best estimate

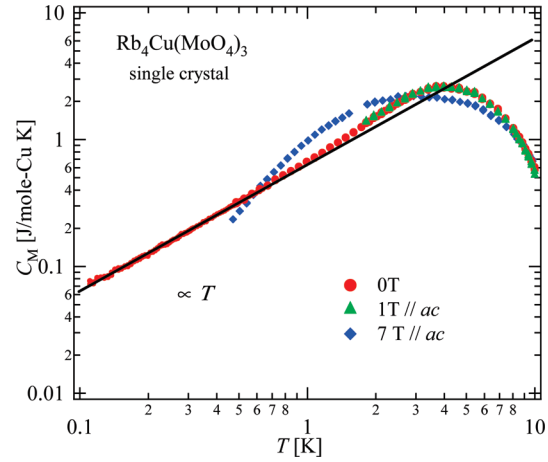

Figure 7. Temperature dependence of the magnetic specific heat of $Rb_4Cu(MoO_4)_3$ at various fields on a full logarithmic scale. Red, green, and blue solid symbols are the results for μ_0H||ac at 0, 1, and 7 T, respectively.

of the lattice specific heat of $Rb_4Cu(MoO_4)_3$. Thus, while the high-temperature estimate of C_M might have a slight systematic error, the discussion below on the most interesting low-temperature part below 3 K, where the lattice contribution is relatively small, should be independent of the estimate. No anomaly indicative of long-range order was observed down to 0.1 K, despite the Weiss constant of $|\Theta_W| \approx 5.0$ K. This is most likely because strong one-dimensionality of the spin structure significantly enhances the spin fluctuations and suppresses the magnetic order, stabilizing the quantum disordered state. The magnetic heat capacity C_M/T forms a broad peak at ~2.5 K, as shown in Figure 6, signaling the development of antiferromagnetic correlation. As has been seen in other Heisenberg antiferromagnetic chain systems,[31] C_M exhibits a linear temperature dependence below 0.8 K under zero magnetic field (Figure 7). At $T < 0.8$ K, C_M/T remains almost constant at $\gamma \approx 0.64$ J/mol·K^2 as $T \rightarrow 0$. For 1-d spin chain systems, it is generally expected that the field with the energy scale lower than the peak temperature of C_M/T (in our case, ~3 T) does not change the linear temperature dependence of the specific heat, but the one beyond the peak temperature scale opens the Zeeman gap in the spin excitation spectrum and thus suppresses the linear dependence. Indeed, we observe that a magnetic field of 1 T does not change the temperature dependence, but 7 T is enough to suppress the peak temperature down to 1.5 K, and thus the specific heat is no longer linear with temperature under 7 T.

Here, we compare our results with the exact solutions available for thermodynamics of the $S = 1/2$ antiferromagnetic Heisenberg chain.[32−34] First, the susceptibility is theoretically estimated to be $x_{th}^{max}J/Ng^2\mu^2 = 0.1469279(1)$ at the peak temperature $T_{th}^{max} = 0.6408510(4)J$. Consequently, one can obtain a J-independent parameter, $\chi_{th}^{max}T_{th}^{max} = 0.0353229(3)g^2$ emu/mol. Using experimentally obtained $g_{ac} = 2.21$, $\chi_{th}^{max}T_{th}^{max}$ is estimated to be 0.1725 emu/mol, which is close to the experimental value $\chi_{ex}^{max}T_{ex}^{max} = 0.155$ emu/mol at $\mu_0H = 0.01$ T for μ_0H||ac (Figure 4). Second, the peak position of the specific

(30) Griffiths, R. B. *Phys. Rev.* **1964**, *133*, A768.
(31) Belik, A. A.; Azuma, M.; Takano, M. *J. Solid State Chem.* **2004**, *177*, 883–888.
(32) Johnston, D. C.; Kremer, R. K.; Troyer, M.; Wang, X.; Klumper, A.; Bud'ko, S. L.; Panchula, A. F.; Canfield, P. C. *Phys. Rev. B* **2000**, *61*, 9558–9606.
(33) Klumper, A.; Johnston, D. C. *Phys. Rev. Lett.* **2000**, *84*, 4701–4704.
(34) Shiroishi, M.; Takahashi, M. *Phys. Rev. Lett.* **2002**, *89*, 117201.

heat by Padé approximations locates at $C_{th}^{max}R = 2.9075$ J/mol·K and $T_{th}^{max} = 4.8$ K for $\mu_0H = 0$ T, where $J = 10.0$ K was used and R is the molar gas constant. These are again close to the experimental values for the specific heat as shown in Figure 6, namely $C_{ex}^{max} = 2.6436$ J/molCu·K at $T_{ex}^{max} = 4.0$ K. Finally, the Wilson−Sommerfeld ratio R_W for the $S = 1/2$ antiferromagnetic Heisenberg chain is given by the equation $R_W(t) = 4\pi^2\chi^*(t)t/3C(t)$, where the spin susceptibility $\chi^*(t)$, the magnetic specific heat $C(t)$, and t are defined as $\chi J/Ng^2\mu_B^2$, CJ/Nk_B^2T, and k_BT/J, respectively.[29] Theoretically, R_W for the $S = 1/2$ antiferromagnetic Heisenberg chain is expected to be exactly 2 for $t \rightarrow 0$. Experimental values of R_W are estimated to be 2.264 for $\mu_0H\|ac$ and 2.217 for $\mu_0H\|b$ at $t = 0.2$. These are 10% larger than the theoretical values but roughly consistent with the theory. All these observations indicate that the system can be regarded as a $S = 1/2$ Heisenberg chain having a quantum spin disordered state at least down to 0.1 K. This is also consistent with the structure, based on the fact that the hole orbital $d_{x^2-y^2}$ of Cu^{2+} in the CuO_4 square is linked along the a-axis through the p orbital of O^{2-} ions. On the other hand, as we discussed above, the magnetic interchain coupling J' in the ac plane should be weak but must still be finite and may contribute to the low-temperature magnetic properties to some extent. Here, J' couples the nearest-neighbor Cu(II) spins in different chains to form an anisotropic triangular lattice antiferromagnet in the ac plane, namely, in the layer consisting of the CuO_5 square pyramid (Figure 2a). For this type of triangular antiferromagnets with spatially anisotropic exchange couplings, a high-temperature series expansion has been made to estimate the variation of the characteristic parameters of the susceptibility curves as a function of $J/(J+J')$, such as T^{max}/Θ_W, $\chi(4T^{max})/\chi^{max}$, and $T^{max}\chi^{max}/Ag^2$ ($A = N_Ag^2\mu_B^2/4k_B = 0.0938$ in cgs units).[35] Using the $\chi(T)$ results at 0.1 T (Figure 4), these parameters are found to be 1.05, 0.56, and 0.35 for $\mu_0H\|ac$ and 1.02, 0.57, and 0.37 for $\mu_0H\|ab$, respectively, thus yielding the estimate of $J/(J + J') \approx 0.95$, namely $J'/J \approx 0.05$, according to the theory. This suggests that the interchain coupling is actually weak, as expected from the crystal structure. Therefore, $Rb_4Cu(MoO_4)_3$ can be regarded as a nearly ideal 1-d antiferromagnetic Heisenberg system.

For $Rb_4Zn(MoO_4)_3$, the specific heat measurement was carried out, and its temperature dependence is shown in Figure 8. No structural phase transition is observed down to 1.8 K, consistent with the results of crystal structure analysis. As we mentioned above, we used this system as a reference material to obtain the lattice contribution to the total specific heat in $Rb_4Cu(MoO_4)_3$. Our detailed structural studies of a quantum low-dimensional magnet, $Rb_4Cu(MoO_4)_3$, indicate that a Cu(II) network separated by a MoO_4 layer forms a 1-d chain of $S = 1/2$ spin. Furthermore, we have found a quantum spin liquid-like feature at low temperature above 0.1 K, consistent with 1-d network of $S = 1/2$ spin.

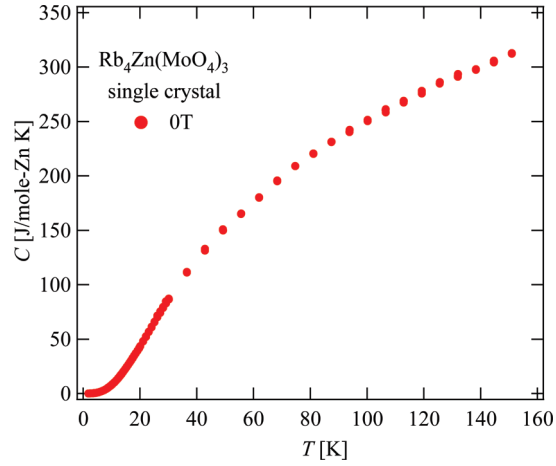

Figure 8. Temperature dependence of the total specific heat of $Rb_4Zn(MoO_4)_3$.

Conclusion

In this article, we report a new one-dimensional quantum antiferromagnet, $Rb_4Cu(MoO_4)_3$, and its nonmagnetic reference, $Rb_4Zn(MoO_4)_3$. Our structural analysis using single crystals of $Rb_4Cu(MoO_4)_3$ strikingly clarifies that the layered compound consists of 1-d chains of Cu^{2+} $S = 1/2$ on each layer because of the anisotropic hybridization between Cu 3d and O 2p orbitals. The low-temperature physical properties are fully consistent with the theoretical expectation for a quantum spin chain system. This indicates that the strong quantum effect enhanced by the low dimensionality stabilizes a quantum paramagnetic state below ~1 K, at least down to 0.1 K, which is 100 times smaller than the nearest-neighbor coupling J. This material may well serve as a model system to deepen our understanding of quantum critical magnetism expected in 1-d spin chains (such as spin-on excitations) through future experiments.

Acknowledgment. J.Y.C. acknowledges NSF Grant DMR 0756281 and the Alfred P. Sloan Fellowship for partial support of this project. This work is partially supported by Grant-in-Aid (No. 21684019) from the Japanese Society for the Promotion of Science, and also by Grant-in-Aid for Scientific Research on Priority Areas (No. 19052003) from the Ministry of Education, Culture, Sports, Science and Technology, Japan.

Supporting Information Available: Selected bond distances and angles and additional crystallographic information, including crystallographic information files (CIF). This material is available free of charge via the Internet at http://pubs.acs.org.

JA100077V

(35) Zheng, W.; Singh, R. R. P.; McKenzie, R. H.; Coldea, R. *Phys. Rev. B* **2005**, *71*, 134422.
(36) Beattie, J. A. *J. Math. Phys.* **1926/1927**, *6*, 1.